Accepted Manuscript

Photoelectrochemical DNA biosensor based on g-C_3N_4/MoS_2 2D/2D heterojunction electrode matrix and co-sensitization amplification with CdSe QDs for the sensitive detection of ssDNA

Pan-Pan Li, Xing-Pei Liu, Chang-Jie Mao, Bao-Kang Jin, Jun-Jie Zhu

PII: S0003-2670(18)31167-X

DOI: 10.1016/j.aca.2018.09.063

Reference: ACA 236299

To appear in: *Analytica Chimica Acta*

Received Date: 9 September 2018

Revised Date: 20 September 2018

Accepted Date: 26 September 2018

Please cite this article as: P.-P. Li, X.-P. Liu, C.-J. Mao, B.-K. Jin, J.-J. Zhu, Photoelectrochemical DNA biosensor based on g-C_3N_4/MoS_2 2D/2D heterojunction electrode matrix and co-sensitization amplification with CdSe QDs for the sensitive detection of ssDNA, *Analytica Chimica Acta* (2018), doi: https://doi.org/10.1016/j.aca.2018.09.063.

Photoelectrochemical DNA biosensor based on g-C_3N_4/MoS_2 2D/2D heterojunction electrode matrix and co-sensitization amplification with CdSe QDs for the sensitive detection of ssDNA

Pan-Pan Li[a,b], Xing-Pei Liu[a], Chang-Jie Mao[*, a], Bao-Kang Jin[a], Jun-Jie Zhu[*, b]

[a] AnHui Province Key Laboratory of Chemistry for Inorganic/Organic Hybrid Functionalized Materials, School of Chemistry and Chemical Engineering, Anhui University, Hefei 230039, P. R. China

[b] State Key Laboratory of Analytical Chemistry for Life Science, School of Chemistry and Chemical Engineering, Nanjing University, Nanjing 210023, P. R. China

*Corresponding author

Chang-Jie Mao, E-mail: maochangjie@sina.com; Tel & Fax: +86 55163861260.
Jun-Jie Zhu, E-mail: jjzhu@nju.edu.cn.

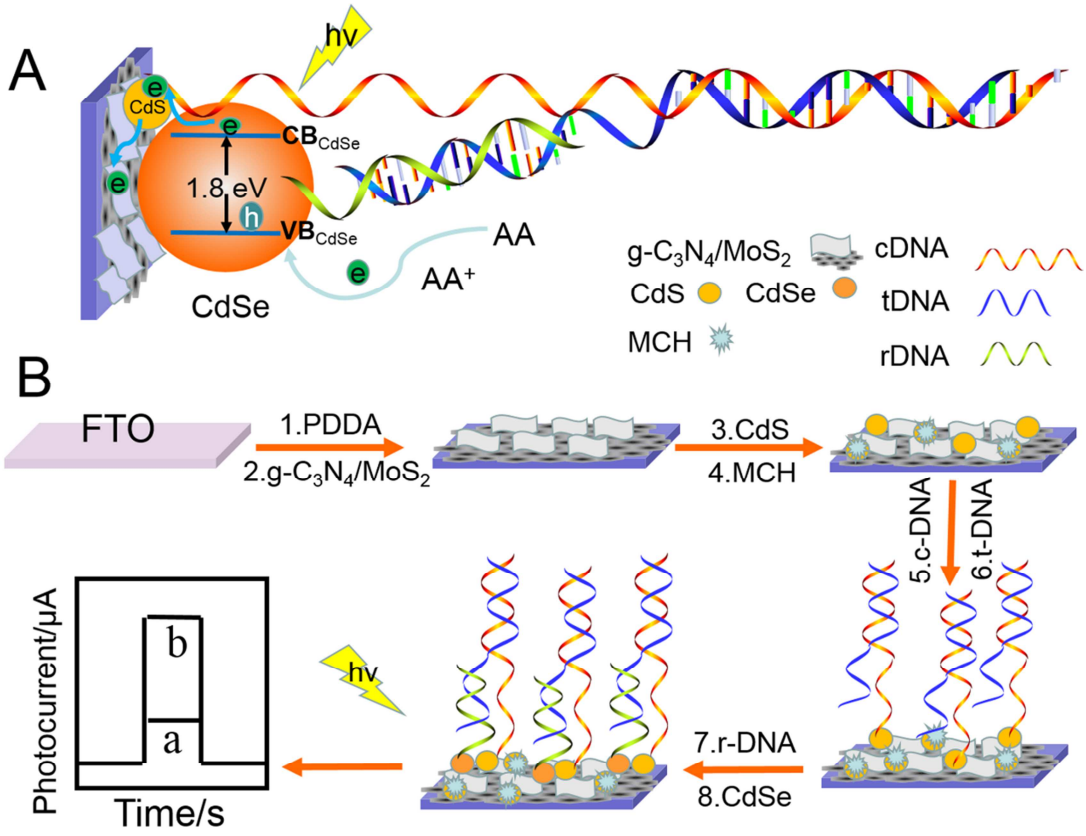

A novel enhanced photoelectrochemical DNA biosensor, based on a compact heterojunction g-C_3N_4/MoS_2 and co-sensitization effect with CdSe QDs, was proposed for analysis of a short ssDNA.

Photoelectrochemical DNA biosensor based on g-C_3N_4/MoS_2 2D/2D heterojunction electrode matrix and co-sensitization amplification with CdSe QDs for the sensitive detection of ssDNA

Abstract

A novel enhanced photoelectrochemical (PEC) DNA biosensor, based on a compact heterojunction g-C_3N_4/MoS_2 and co-sensitization effect with CdSe quantum dots (QDs), was first proposed for simple and accurate analysis of a short ssDNA. In this work, the g-C_3N_4/MoS_2 was successfully synthesized and used as the electrode matrix material to construct PEC biosensor for the first time. As expected, 2D/2D heterojunction was formed between g-C_3N_4 and MoS_2, which could promote the separation of photogenerated electron-hole pairs resulting in an enhanced photocurrent. In the present of target DNA, the CdSe QDs labeled reporter DNA was complementary pairing with target DNA which was specific recognized by capture DNA loading on self-assembled CdS QDs film, leading to close contact between CdSe QDs and g-C_3N_4/MoS_2 modified electrode surface, thereby resulting in the enhance photocurrent intensity due to the co-sensitization effect. Under the optimal operating conditions, the photoelectrochemical biosensor demonstrated favorable accuracy and could responds to 0.32 pM (S/N=3) with a linear concentration ranging from 1.0 pM to 2.0 μM. Moreover, the proposed PEC DNA biosensor exhibits high sensitivity, excellent specificity, acceptable reproducibility and accuracy, showing a promising potential in DNA bioanalysis and other relative fields.

Keywords: Photoelectrochemical, g-C_3N_4, MoS_2, Heterojunction, CdSe quantum dots, Co-sensitive.

1. Introduction

Photoelectrochemical (PEC) method as a recent but rapidly developing analytical technique has been extensively employed in the life science analysis. The PEC biosensor with total separation of excitation (visible light) and detection (photogenerated electron) modes showing reduced background takes responsibility for its remarkable sensitivity and gives a preeminent alternative to other traditional electrochemical and optical methods [1-4]. Moreover, it's other superiorities such as simple operation, cheap instrumentation, and wide calibration ranges result in the widespread attention of PEC biosensor. In general, the photoelectric transformation efficiency of photoactive materials utilized to construct PEC biosensor largely determines its analytical performance [5-7]. Therefore, the work that trying to find a suitable photoactive material for PEC detection assay is necessary and meaningful.

Currently, graphite-like carbon nitride (g-C_3N_4), a π-conjugated semiconductor with unique electronic structure [8-10], has become a research hotspot. It is nontoxic, inexpensive, easy synthesis and chemically stable, and has already played an important role in water splitting [11-13], energy conversion and storage [14-16], lithium-ion battery [17], and electrogenerated chemiluminescence applications [18]. Although there are some successful examples of the application of g-C_3N_4, its lower separation capability of the photoinduced electron-hole pairs greatly restricts its practical usage [19]. To circumvent this problem, many methods have been proposed, for instance nonmetal doping [20-22], metal deposition [23], and designing heterojunction structures [24-26]. Among them, heterogeneous coupling can be more efficient for PEC detection. As for g-C_3N_4, a two-dimensional (2D) material, it can form three types of heterostructures, namely, 2D/2D, 1D/2D, and 0D/2D, with the

2D/2D heterojunction revealing the greatest efficiency because the layered junction cut down the diffusion distance and shorten the reaction time, which accelerate the efficiency of photoinduced carriers and enhance the PEC performance [27]. Hence, it is essential to find a 2D nanomaterial to couple with g-C_3N_4 nanosheet and form a planar heterojunction to enhance the photocurrent response.

Molybdenum disulfide (MoS_2) is a type of layered quasi-2D chalcogenide material, with perfect light absorption coefficient [28] and large photoexcited carrier lifetimes [29]. The monolayer MoS_2 exhibits a structure of two hexagonal S atoms, and that are connected to the hexagonal plane of Mo atom by covalent bond. In the bulk, single MoS_2 layers are connected each other by weak van der Waals force with a narrow band gap of about 1.3 eV, and the direct band gap of the single layer MoS_2 is about 1.8 eV [30, 31]. All of these properties proves it is a perfect semiconductor material suitable for photodetector [31,32] and light emitter applications [33]. In addition, MoS_2 has similar structure to g-C_3N_4, and it can decrease the different lattice parameters and promote the planar growth of g-C_3N_4 surface [28]. Thus, it is feasible to bridge MoS_2 with g-C_3N_4 to build a 2D/2D heterojunction, which not only expand the surface area but accelerate the transfer of electrons and enhance the photoelectric property.

It is universally known that different semiconductor materials can absorb different wavelength ranges of lights because of their diverse inherent binding gaps. Therefore, cosensitized structures obtained by coupling large band gap semiconductors with narrow band-gap ones are catching the researcher’s eyes. Among which, CdSe QDs semiconductors with an extremely narrow band gap about 1.8 eV are widely utilized as co-sensitive material to enhance the photo-to-current efficiency

[34]. Therefore, we designed the DNA analysis strategy based on the co-sensitization amplification effect of CdSe QDs for highly sensitive detection of single-stranded DNA (ssDNA).

In this work, we chose ssDNA sequence, a common HTLV-II DNA in human T-cell lymphotropic virus type II closely associated with pulmonary and urinary tract symptoms, as target analyte (t-DNA). The photocurrent induced mechanism of the DNA assay were shown in Scheme 1A. We build a 2D/2D heterojunction between MoS_2 with g-C_3N_4 to promote the separation of photogenerated electron-hole pairs and resulting in an enhanced and stable photocurrent. Then CdSe QDs were act as co-sensitive materials to broaden the light absorb rang. Upon the light irradiation, the CdSe QDs generated electron hole pairs and the electron were flow from the conductive band to the surface of g-C_3N_4/MoS_2 and finally get to the fluorine-doped tin oxide (FTO) electrode. The hole were leaved on the valence band, and in order to prevent the electron recombination, the test solution were supported by ascorbic acid (AA). The detailed fabrication process of the PEC biosensor is described in Scheme 1B. Here, we coupled MoS_2 with g-C_3N_4 to form 2D/2D heterostructures, and then g-C_3N_4/MoS_2 with negatively charge was assembled on the FTO electrode pre-treated with positively charged poly dimethyl diallyl ammonium chloride (PDDA) through the electrostatic attraction. After it dried naturally, CdS QDs were doped on the surface of g-C_3N_4/MoS_2 by covalent bonds (Cd-S) to serve as an efficient platform for further bio-function with thiol group terminated capture DNA (c-DNA) due to forceful Cd-SH bonds. After we blocked the unbound sites with

6-hydroxy-1-hexanethiol (MCH), nanocomposites g-C_3N_4/MoS_2/CdS QDs were successfully constructed and acted as the PEC matrix with dramatic photocurrents for the sensitivity detection of ssDNA. In the present of target DNA, the CdSe QDs labeled reporter DNA was complementary pairing with target DNA which was specific recognized by capture DNA loading on self-assembled CdS QDs film, leading to close contact between CdSe QDs and g-C_3N_4/MoS_2 modified electrode surface, thereby resulting in an enhanced photocurrent signal response with increasing analyte concentration due to the co-sensitization effect. In addition, the proposed platform exhibits high sensitivity, excellent specificity, acceptable reproducibility and accuracy, showing a promising potential to monitor the DNA activity and diagnose DNA relevant clinical diseases.

2. Experimental

2.1 Fabrication of FTO/PDDA/g-C_3N_4/MoS_2/CdS QDs electrode

Firstly, the FTO electrodes were cleaned with deionized water, acetone and ethanol by sonication for 20 min, respectively, and then dried at an oven overnight. The FTO glass was sheared into square ones with an area of 45 mm^2.Afterwards, 30 μL PDDA (2%) was dropped on the FTO electrode for 1 h to make the surface get positive charges. The fixed area was washed by PBS (0.01 M) and dried by pure N_2. After that, 20 μL g-C_3N_4 with MoS_2 compounds, which mixed by physical oscillation (the volume ratio of MoS_2 and g-C_3N_4 was 3), were deposited on the fixed area. After airing, 15 μL CdS QDs were modified on the glass at environment temperature. Finally, the FTO/PDDA/g-C_3N_4/MoS_2/CdS QDs electrode was obtained (The synthesis methods of g-C_3N_4, MoS_2 and CdS QDs were shown in the supporting information).

2.2 Fabrication of DNA biosensor

Under normal conditions, 30 μL of 1 μM c-DNA was preprocessed with 10 mM Tris-(2-carboxyethyl)-phosphine (TCEP) for 1 h to break disulfide bond and then incubated with FTO/PDDA/g-C_3N_4/MoS_2/CdS QDs electrode at 4 °C for overnight. Then the electrode was washed by TE buffer (10 mM Tris-HCl, 1 mM EDTA, PH=8.0) and incubated with 30 μL of 1 mM MCH for 1 h at 37 °C, which was aimed to detach the unattached c-DNA and cover the unbound sites. 30 μL t-DNA with different concentrations was complemented for 100 min at 37 °C. Then, the electrode was washed by TE buffer which incubated with 30 μL r-DNA and then modified by CdSe QDs (containing 40 mg mL^{-1} EDC and 10 mg mL^{-1} NHS) at 37 °C for 120 min. The r-DNA could be connected to CdSe QD_S by EDC-NHS coupling reactions between the amino groups of rDNA and carboxyl groups of CdSe QDs. The obtained electrode was detected by PEC test after washing with PBS buffer (pH=7.4) (The synthesis method of CdSe QDs was shown in the supporting information).

2.3 PEC Measurement

PEC detection was tested in PBS (0.1 M, pH=7.4, Na_2HPO_4, NaH_2PO_4, NaCl) containing 0.1 M AA which act as a good electron donor in the PEC test. The Xenon lamp with a wave length from 280 to 1000 nm served with as the excitation source.

3. Results and discussion

3.1 Characterization of materials

The crystal-phase properties of MoS_2 and g-C_3N_4 were served by XRD measurement. Figure 1A shows that all diffraction peaks can be associated with the hexagonal wurtzite structure of MoS_2 (JCPDS, No. 37-1492). The films display broad diffraction peaks whose value of 2θ was 14.8°, 33.5°, 39.5°, 49.8°, and 58.3°, corresponding to the (002), (101), (103), (105), and (110) planes of anatase MoS_2, respectively,

indicating that MoS_2 nanosheeets were obtained. The g-C_3N_4 sample (JCPDS No. 50-1250) has two strong diffraction peaks at about 13.1° and 27.4°, which are characteristic of (100), (002) planes. The representative SEM image shows in Figure 1B that g-C_3N_4 has a good cooperation with MoS_2 nanosheet at the volume ratio of 3, thus, the heterostructures formed between the 2D/2D interface, which is known to be highly useful for the separation of electron transfer and photoinduced electron-hole pairs. Moreover, it also supplies a large area for the modification of CdS QDs. The SEM images of volume ratio of 1, 2, 3, 4 (Figure S1 a-d) were provided in the supporting information.

3.2 XPS analysis

The chemical states of MoS_2, g-C_3N_4, and g-C_3N_4/MoS_2 nanocomposites were analyzed by X-ray photoelectron spectroscopy (XPS). In Figure 2a, the C1s spectra 284.9 and 289.2 eV for g-C_3N_4 are the SP^2 C-C bonds of graphitic carbon and the sp^2-hybridized carbons in the triazine rings (N-C=N) respectively [35]. However, those peaks in the g-C_3N_4/MoS_2 shifted to 284.8 and 288.5 eV which may be because of the intense interface interaction. Figure 2b contains three peaks with binding energies at 398.65, 400.15 and 405.25 eV, which can be related to C-N-C, N-$(C)_3$ and N-H, respectively [36]. As shown in Figure 2c, two main peaks at 228.95 and 232.30 eV are well related to Mo (+4) 3d3/2 and Mo (+4) 3d5/2, respectively. Figure 2d shows that the peaks at 161.7 and 163.1 eV are corresponding to S2p3/2 and S2p1/2 which are according with the S^{2-} in MoS_2 [37]. The XPS results confirmed the co-existence of g-C_3N_4 and MoS_2 and the shift of binding energy also indicated the heterojunction between g-C_3N_4 and MoS_2 were successfully formed.

3.3 TEM and high-resolution TEM (HRTEM) analyses

The microstructures of g-C_3N_4 and g-C_3N_4/MoS_2 were examined by transmission electron microscopy (TEM) and high resolution transmission electron microscopy (HRTEM), as shown in Figure 3. The TEM image of Fig 3a shows g-C_3N_4 with a lamellar nanosheet structure. Figure 3b shows the HRTEM of g-C_3N_4, indicating that it has a thin nature. Figure 3c shows a representative TEM image of MoS_2/g-C_3N_4. The MoS_2 nanocrystals are tiled on the surface of g-C_3N_4 nanocrystals with the lattice distance (Figure 3d) of 0.28 nm, related to the (100) planes of bulk MoS_2, which indicates a 2D/2D heterojunction were successfully formed between g-C_3N_4/MoS_2 interface.

3.4 Characterization of CdS and CdSe QDs

Figures S2 shows HRTEM and UV-visible results of the synthesized CdS and CdSe QDs, respectively. As shown in Figure S2A and B, they both have clear lattice fringes with average sizes of 4.28 and 3.01 nm, respectively. Figure S2C is the UV image where the CdS QDs have an absorption peak at 370 nm and CdSe QDs at 445 nm.

3.5 Electrochemical impedance spectroscopy (EIS) characterization of DNA biosensor

As a beneficial method for displaying characteristic of electrode, EIS spectra applied to display the procedure stage of the DNA biosensor. As shown in Figure 4A, it consists of two parts, the semicircle diameter which detected at higher frequencies presented the limited process for electron-transfer resistance (R_{et}) and the linear part which got at lower frequencies symbolized the diffusion limited process. The FTO/g-C_3N_4/MoS_2 electrode reveals a relatively small R_{et} value, which is significantly increased by modified CdS QDs and the changes may because of the separation of photoinduced electron holes pairs and the rapid charge transfer from the surface of FTO/g-C_3N_4/MoS_2 to the surface of CdS QDs [38]. With the further

modification of c-DNA and MCH, the R_{et} increases obviously (curve c). This is due to the low conductivity of the c-DNA sequence and MCH molecules, and the electrostatic repulsion between the negative charge of the DNA and the $Fe(CN)_6^{3-/4-}$ redox probe [39]. The R_{et} value is marginally increased for modified t-DNA (curve d) because of the small conductivities between DNA strands. After modification of the CdSe QDs, the R_{et} value exhibits a remarkable increase, which is similar to curve b compared with curve a. The significant change of R_{et} indicates the successful manufacture of the DNA biosensor.

3.6 PEC performance of DNA biosensor

Several procedures were used to examine the PEC performance of the DNA biosensor. As shown in Figure 4B, the photocurrent of the g-C_3N_4/CdS modified FTO is 9.9 μA (curve a). When g-C_3N_4 is combined with MoS_2, the photocurrent of g-C_3N_4/MoS_2/CdS electrode increases to 18.9 μA (curve b) because g-C_3N_4 and MoS_2 can form an effective heterojunction extending the light absorption range. The photocurrent drops to 10.1 μA (curve c) after the modification of the c-DNA and MCH, which explains the weak charge-transfer abilities both of t-DNA and MCH. Moreover, the photocurrent decreases to 4.9 μA (curve d) with the t-DNA modification. This means the charge transfer between DNA is very slow, so we use CdSe QDs to amplify the photocurrent. After p-DNA/CdSe QDs are bound to the electrode, the photocurrent intensity increases to 32.8 μA (curve e). It can be explained for the high-efficient sensitization of the CdSe QDs. These results show that the DNA biosensor is successfully developed.

3.7 Optimal conditions of DNA biosensor

Figure S1a and b show the photocurrent of the FTO/g-C_3N_4/MoS_2 electrode modified with different volumes and ratios of the g-C_3N_4 and MoS_2 nanosheet suspension.

When the FTO/g-C_3N_4/MoS_2 absorbed the light, the photocurrent intensively increased, and the photocurrent intensity was changed with the change of the volume ratio. We selected the volume ratio as three (MoS_2/g-C_3N_4) and the suspension volume reached to 20 μL. The fabricated FTO/g-C_3N_4/MoS_2 electrode possessed the maximum photocurrent intensity. As the volume of g-C_3N_4/MoS_2 increased, the surface recombination potentially increased and the diffusion resistance increased, therefore, the optical current intensity decreased gradually [40]. Hence, the conditions that the volume ratio of three (MoS_2/g-C_3N_4) and 20 μL suspension were used to fabricate the electrode. We also made other optimizations (Figure S1c-e) to improve our experimental setup, such as the volume of CdS QDs, the incubation time of CdSe QDs and DNA hybridization time. Finally, we chose the optimal conditions that the volume of CdS was 15 μL, and the time of t-DNA hybridization was 100 min, and the CdSe QDs incubation time was 120 min.

3.8 PEC detection

The signal amplification of PEC DNA detection is based on DNA hybridization. The photocurrent signal is directly related to the t-DNA concentration. Figure 5A displays the photocurrent signal of the PEC DNA biosensor incubated with different concentrations of t-DNA. The photocurrents increases gradually by elevating the concentration of t-DNA. As shown in Figure 5B, the photocurrent signal is linearly related to 1 pM to 2 μM. The regression equation is $I\ (\mu A) = 14.2494 + 1.2061\ log_{10}C_{DNA}\ (\mu M)$ and the correlation is 0.995. The detection limit (S/N=3) for the target DNA is estimated to be 0.32 pM. The sensitivity of our DNA assay is also compared with other previous PEC reports, and the results are shown in Table 1. Our PEC DNA biosensor provides a better detection limit and a wider linear response scope.

Therefore, the control experiment also proves a photocurrent signal amplification strategy.

3.9 Selectivity, repeatability, and stability of the DNA assay

To evaluate the selectivity of the PEC assay, some comparison involving t-DNA (a), one-base mismatch DNAI (b), three-base mismatch DNAII (c), and non-complementary DNA (d) were made under the uniform concentration (2 μM). As shown in Figure 6, the photocurrent of t-DNA reveals an obvious increase compared to the others. The signal of photocurrents indicate that the t-DNA and DNA_2 have a selective hybridization. The relative standard deviation for 2 μM, 1 nM and 1 pM of t-DNA were 2.49%, 2.57% and 4.37%, respectively, which indicates good detection reproducibility of the proposed PEC biosensor. We also evaluated the stability of the PEC DNA biosensor. After we stored the working electrodes at 4 °C for over 2 weeks, the average photocurrent of electrode is 99.4% of the original value, implying its perfect storage stability.

4. Conclusion

In this study, we developed an enhanced PEC genosensor for highly sensitive and accurate analysis of ssDNA based on a compact 2D heterojunction g-C_3N_4/MoS_2 and co-sensitization effect with CdSe QDs. The electrode matrix was constructed with g-C_3N_4/MoS_2, as expected, accompanying an effective 2D heterojunction. The XPS spectrums clearly demonstrate the existence of 2D heterojunction, and other characterization methods including XRD, TME, SEM and EIS were utilized to explain the successful synthesis of the materials and manufacture of the PEC genosensor. The co-sensitization amplification effect between CdSe QDs and g-C_3N_4/MoS_2 was smartly exploited to design a novel DNA analysis strategy. This enhanced PEC genosensor was well fabricated and exhibited high sensitivity,

excellent specificity, and acceptable reproducibility and accuracy. This work provides a novel and alternative avenue to construct PEC genosensing platforms to monitor the DNA activity and diagnose DNA relevant clinical diseases.

Acknowledgements

References

[1] Y.N. Zheng, W.B. Liang, C.Y. Xiong, Y. Zhuo, Y.Q. Chai, R. Yuan, Universal ratiometric photoelectrochemical bioassay with target-nucleotide transduction-amplification and electron-transfer tunneling distance regulation strategies for ultrasensitive determination of microRNA in cells, Anal. Chem. 89 (2017) 9445-9451.

[2] Z.L. Qiu, J. Shu, D.P. Tang, Near-infrared-to-ultraviolet light-mediated photoelectrochemical aptasensing platform for cancer biomarker based on core-shell $NaYF_4$:Yb, Tm@TiO_2 upconversion microrods, Anal. Chem. 90 (2018) 1021-1028.

[3] W.W. Zhan, Q. Kuang, J.Z. Zhou, X.J. Kong, Z.X. Xie, L.S. Zheng, Semiconductor @ metal-organic framework core-shell heterostructures: A case of ZnO @ ZIF-8 nanorods with selective photoelectrochemical response, J. Am. Chem. Soc. 135 (2013) 1926-1933.

[4] W.W. Zhao, J.J. Xu, H.Y. Chen, Photoelectrochemical bioanalysis: The state of the art, Chem. Soc. Rev. 44 (2015) 729-741.

[5] S.Z. Lv, K.Y. Zhang, Y.Y. Zeng, D.P. Tang, Double photosystems-based 'Z-Scheme' photoelectrochemical sensing mode for ultrasensitive detection of disease

biomarker accompanying three-dimensional DNA walker, Anal. Chem. 90 (2018) 7086-7093.

[6] B. Zhang, L. Lu, Q. Hu, F. Huang, Z. Lin, ZnO nanoflower-based photoelectrochemical DNAzyme sensor for detection of the detection of Pb^{2+}, Biosens. Bioelectron. 56 (2014) 243-249.

[7] J. Huang, Y.R. Wu, Y. Chen, Z. Zhu, X.H. Yang, C.Y.J. Yang, K.M. Wang, W.H. Tan, Pyrene-excimer probes based on the hybridization chain reaction for the detection of nucleic acids in complex biological fluids, Angew. Chem. Int. Ed. 123 (2011) 421-424.

[8] L.W. Zhang, H.B. Fu, Y.F. Zhu, Efficient TiO_2 photocatalysts from surface hybridization of TiO_2 particles with graphite-like carbon, Adv. Funct. Mater. 18 (2010) 2180-2189.

[9] H. Zhang, R. Zong, Y.F. Zhu, Photocorrosion inhibition and photoactivity enhancement for zinc oxide via hybridization with monolayer polyaniline, J. Phys. Chem. C 113 (2014) 4605-4611.

[10] K.Y. Zhang, S.Z. Lv, Z.Z. Lin, D.P. Tang, CdS:Mn quantum dot-functionalized g-C_3N_4 nanohybrids as signal generation tags for photoelectrochemical immunoassay of prostate specific antigen coupling DNAzyme concatamer with enzymatic biocatalytic precipitation, Biosens. Bioelectron. 95 (2017) 34-40.

[11] Y.P. Zhu, T.Z. Ren, Z.Y. Yuan, Mesoporous phosphorus-doped g-C_3N_4 nanostructured flowers with superior photocatalytic hydrogen evolution performance, ACS Appl. Mater. Interfaces 7 (2015) 16850-16856.

[12] F. He, G. Chen, Y.G. Yu, S. Hao, Y.S. Zhou, Y. Zheng, Facile approach to synthesize g-PAN/g-C_3N_4 composites with enhanced photocatalytic H_2 evolution activity, ACS Appl. Mater. Interfaces 6 (2014) 7171-7179.

[13] H.J. Shi, G.H. Zhao, M.C. Liu, Z.L. Zhu, A novel photoelectrochemical sensor based on molecularly imprinted polymer modified TiO_2 nanotubes and its highly selective detection of 2,4-dichlorophenoxyacetic acid, Elecom. 13 (2011) 1404-1407.

[14] B. Zhang, L. Lu, Q. Hu, F. Huang, Z. Lin, ZnO nanoflower-based photoelectrochemical DNAzyme sensor for detection of the detection of Pb^{2+}, Biosens. Bioelectron. 56 (2014) 243-249.

[15] X.M. Zhang, L.M. Li, X. Peng, R.S. Chen, K.F. Huo, P.K. Chu, Non-enzymatic hydrogen peroxide photoelectrochemical sensor based on WO_3 decorated core-shell TiC/C nanofibers electrode, Electrochim Acta 108 (2013) 491-496.

[16] Y. Gong, M. Li, Y. Wang, Carbon nitride in energy conversion and storage: recent advances and future prospects, Chem. Sus. Chem. 8 (2015) 931-946.

[17] Z. Meng, Y. Xie, T.W. Cai, Z.X. Sun, K.M. Jiang, W.Q. Han, Graphene-like g-C_3N_4 nanosheets/sulfur as cathode for lithium-sulfur battery, Electrochim Acta 210 (2016) 829-836.

[18] Y.T. Liu, Q.B. Wang, J.P. Lei, Q. Hao, W. Wang, H.X. Ju, Anodic electrochemiluminescence of graphitic-phase C_3N_4 nanosheets for sensitive biosensing, Talanta 122 (2014) 130-134.

[19] Y.J. Wang, R. Shi, J. Lin, Y.F. Zhu, Enhancement of photocurrent and photocatalytic activity of ZnO hybridized with graphite-like C_3N_4, Energy Environ. Sci. 4 (2011) 2922-2929.

[20] G. Dong, K. Zhao, L. Zhang. Carbon self-doping induced high electronic conductivity and photoreactivity of g-C_3N_4, Chem, Commun. 48 (2012) 6178-6180.

[21] Y. Zhu, T. Ren, Z. Yuan, Mesoporous phosphorus-doped g-C_3N_4 nanostructured flowers with superior photocatalytic hydrogen evolution performance, ACS Appl. Mater. Interfaces 7 (2015) 16850-16856.

[22] S.C. Yan, Z.S Li, Z.G. Zou, Photodegradation of rhodamine b and methyl orange over boron-doped g-C_3N_4 under visible light irradiation, Langmuir 26 (2010) 3894-3901.

[23] M. Reza Gholipour, C.T. Dinh, F. Béland, T.O. Do, Nanocomposite heterojunctions as sunlight-driven photocatalysts for hydrogen production from water splitting, Nanoscale 7 (2015) 8187-8208.

[24] Y. He, Y. Zhang, B. Teng, M. Fan, New application of Z-scheme Ag_3PO_4/g-C_3N_4 composite in converting CO_2 to fuel, Environ. Sci. Technol. 49 (2015) 649-656.

[25] W. Liu, M. Wang, C. Xu, S. Chen, Significantly enhanced visible-light photocatalytic activity of g-C_3N_4 via ZnO modification and the mechanism study, J. Mol. Catal. A Chem. 368-369 (2013) 9-15.

[26] Y. He, Y. Wang, L. Zhang, B. Teng, M. Fan, High-efficiency conversion of CO_2 to fuel over ZnO/g-C_3N_4 photocatalyst, Appl. Catal. B: Environ. 168-169 (2015) 1-8.

[27] Z. Zhang, J. Huang, M. Zhang, Q. Yuan, B. Dong, Ultrathin hexagonal SnS_2 nanosheets couple with C_3N_4 nanosheets as 2D/2D heterojunction photocatalysts toward high photocatalytic activity, Appl. Catal. B: Environ. 163 (2015) 298-305.

[28] K.F. Mark, C.G. Lee, J. Hone, J. Shan, T.F. Heinz, Atommically thin MoS_2: A new direct-gap semiconductor, Phys. Rev. Lett. 105 (2010) 136805.

[29] Y. Yao, L. Tolention, Z. Yang, X. Song, W. Zhang, Y. Chen, C.P. Wong, High-conce ntration aqueous dispersions of MoS_2, Adv. Funct. Mater. 23 (2013) 3577-3583.

[30] B. Radisavljevic, A. Radenovic, J. Brivio, V. Giacomtti, A. Kis, Single-layer MoS_2 transistors, Nat. Nanotechnol. 6 (2011) 147-150.

[31] Y. Li, H. Wang, L. Xie, Y. Liang, G. Hong, H. Dai, MoS_2 nanoparticles grown on graphene: an advanced catalyst for the hydrogen evolution reaction, J. Am. Chem. Soc. 133 (2011) 7296-7299.

[32] S. Lebegue, O. Eriksson, Electronic structure of two-dimensional crystals from abinitio theory, Phys. Rev. B 79 (2009) 5409.

[33] A. Splendiani, L. Sun, Y. Zhang, T. Li, J. Kim, C.Y. Chim, G. Galli, F.E. Wang, Merging photoluminescence in monolayer MoS_2, Nano Lett. 10 (2010) 1271-1275.

[34] J. Shu, D.P. Tang, Current advances in quantum-dots-based photoelectrochemical immunoassays, Chem. Asian J. 12 (2017) 2780-2789.

[35] J. Tian, Q. Liu, A.M. Asiri, K.A. Alamry, X. Sun, Ultrathin graphitic C_3N_4 nanosheets/graphene composites: efficient organic electrocatalyst for oxygen evolution reaction, Chem. Sus. Chem 7 (2014) 2125-2130.

[36] Q.Y. Lin, L. Li, S.J. Liang, M.H. Liu, J.H. Bi, L. Wu, Efficient synthesis of monolayer carbon nitride 2D nanosheet with tunable concentration and enhanced visible-light photocatalytic activities, Appl. Catal. B: Environ. 163 (2015) 135-142.

[37] X.Q. Hao, Z.L. Jin, S.X. Min, G.X. Liu, Modulating photogenerated electron transfer with selectively exposed Co-Mo facets on a novel amorphous g-C_3N_4/$Co_xMo_{1-x}S_2$ photocatalyst, RSC Adv. 6 (2016) 23709-23717.

[38] D. Jiang, X. Du, L. Zhou, H. Li, K. Wang, New insights toward efficient charge-separation mechanism for high-performance photoelectrochemical aptasensing: enhanced charge-carrier lifetime via coupling ultrathin MoS_2 nanoplates with nitrogen-doped graphene quantum dots, Anal. Chem. 89 (2017) 4525-4531.

[39] C.X. Li, W. Lu, M. Zhu, B. Tang, Development of visible-light induced photoelectrochemical platform based on cyclometalated Iridium(III) complex for bioanalysis, Anal. Chem. 89 (2017) 11098-11106.

[40] J.A. Anta, E. Guillen, R. Tenazaera, ZnO-based dye-sensitized solar cells, J. Phys. Chem. C 116 (2012) 11413-11425.

Figure captions

Scheme 1. A. mechanism of PEC DNA biosensor.

B. Fabricating steps of PEC DNA biosensor.

Figure 1. (A) XRD patterns of g-C_3N_4 and MoS_2. (B) SEM images of g-C_3N_4, and MoS_2 nanocomposites.

Figure 2. XPS spectrum of g-C_3N_4/MoS_2: (A) C1s, (B) N1s, (C) Mo3d and (D) S2p.

Figure 3. TEM images of (a) g-C_3N_4 and (c) g-C_3N_4/MoS_2. HRTEM images of (b) g-C_3N_4, and (d) g-C_3N_4/MoS_2.

Figure 4. (A) EIS and (B) photocurrent responses of **(**a) g-C_3N_4/CdS QDs, (b) g-C_3N_4 /MoS_2/CdS QDs, (c) g-C_3N_4 /MoS_2/CdS QDs /MCH/c-DNA, (d) g-C_3N_4/MoS_2/CdS QDs/MCH/c-DNA/t-DNA_2, and (e) g-C_3N_4/MoS_2/CdS QDs /MCH/c-DNA/t-DNA_2/r-DNA/CdSe QDs.

Figure 5. (A) Photocurrent responses of PEC DNA biosensor to different concentrations of t-DNA from 1 pM to 2 μM. (B) Calibration curve of the PEC DNA biosensor to t-DNA solution with various concentrations. The error bars display standard deviations of six parallel tests.

Figure 6. Photocurrent responses of the PEC DNA assay to 30 μL of 2 μM different DNA sequences. (a) t-DNA, (b) one-base mismatch DNAI, (c) three-base mismatch DNAII and (d) non-complementary DNA.

Scheme 1

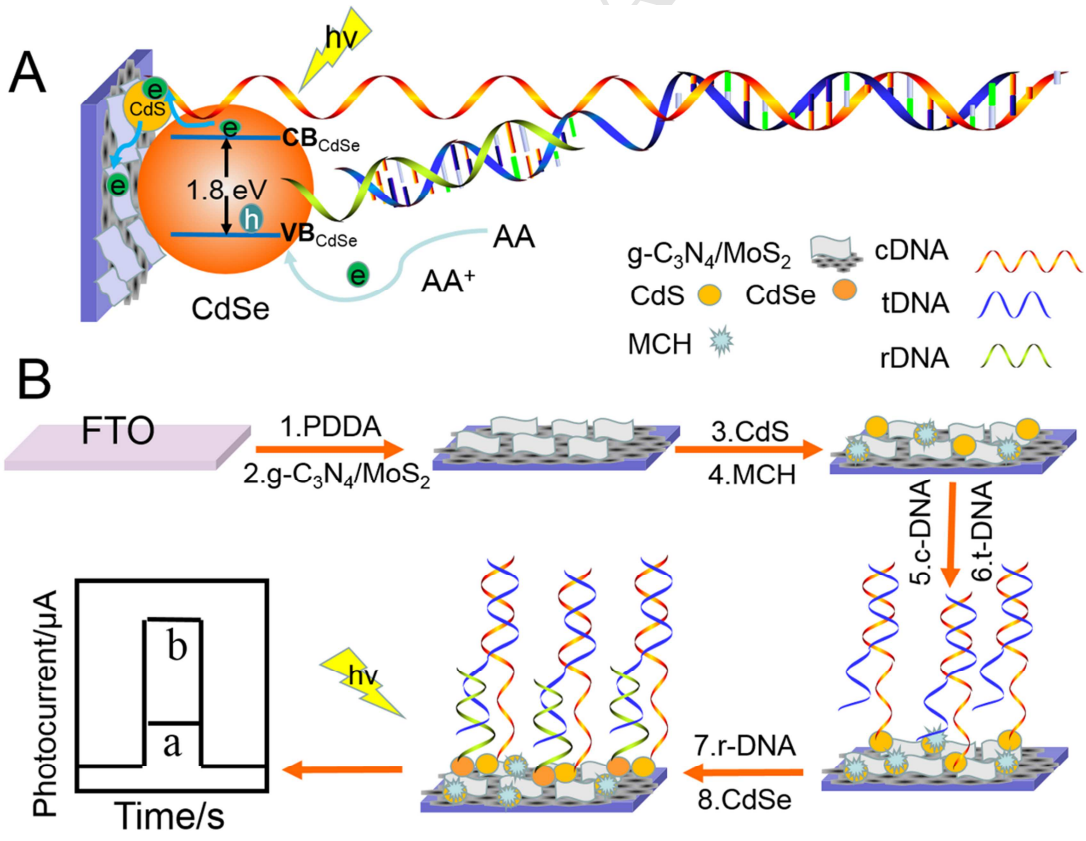

Scheme 1. A. Mechanism of PEC DNA biosensor. **B.** Fabricating steps of PEC DNA biosensor.

Figure 1

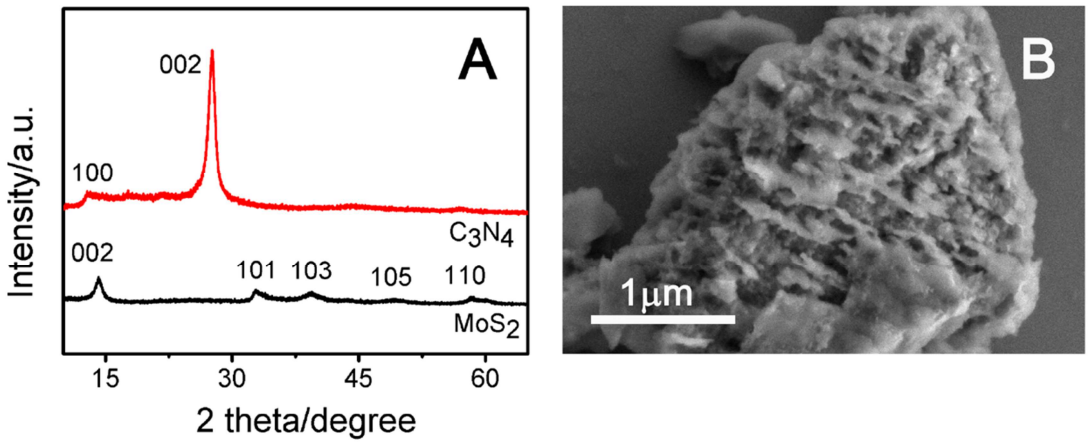

Figure 1. (A) XRD patterns of g-C_3N_4 and MoS_2. (B) SEM images of g-C_3N_4, and MoS_2 nanocomposites.

Figure 2

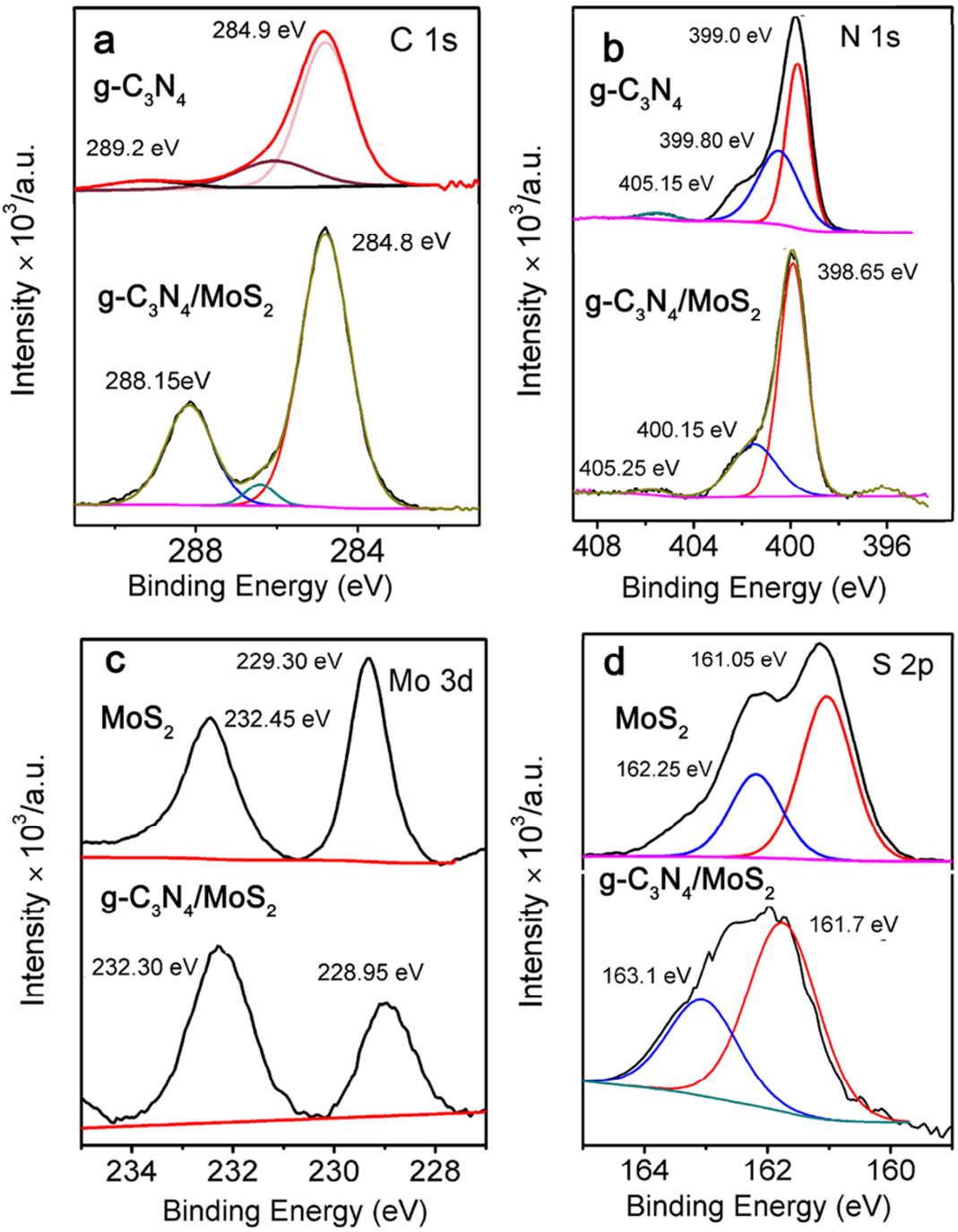

Figure 2. XPS spectrum of g-C_3N_4/MoS_2: (A) C1s, (B) N1s, (C) Mo3d and (D) S2p.

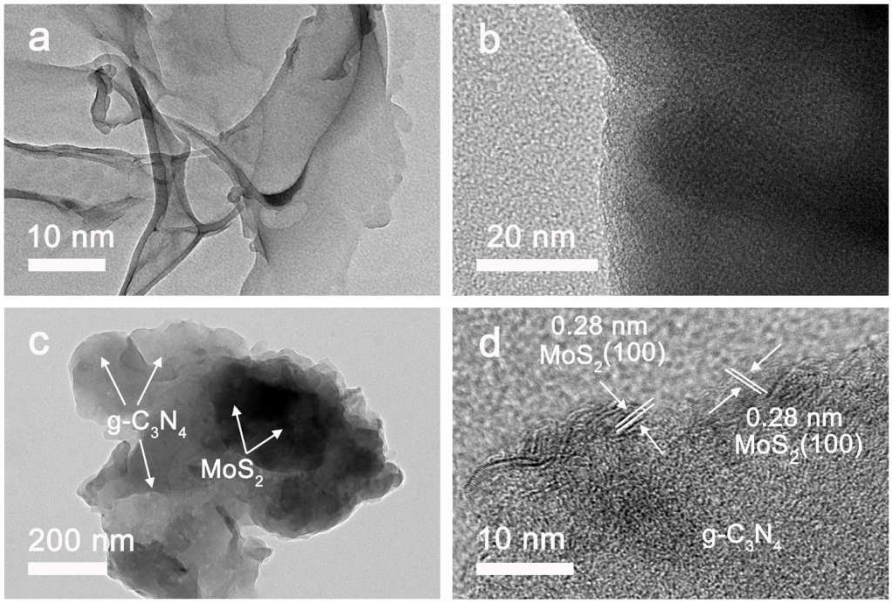

Figure 3

Figure 3. TEM images of (a) g-C_3N_4 and (c) g-C_3N_4/MoS_2. HRTEM images of (b) g-C_3N_4, and (d) g-C_3N_4/MoS_2.

Figure 4

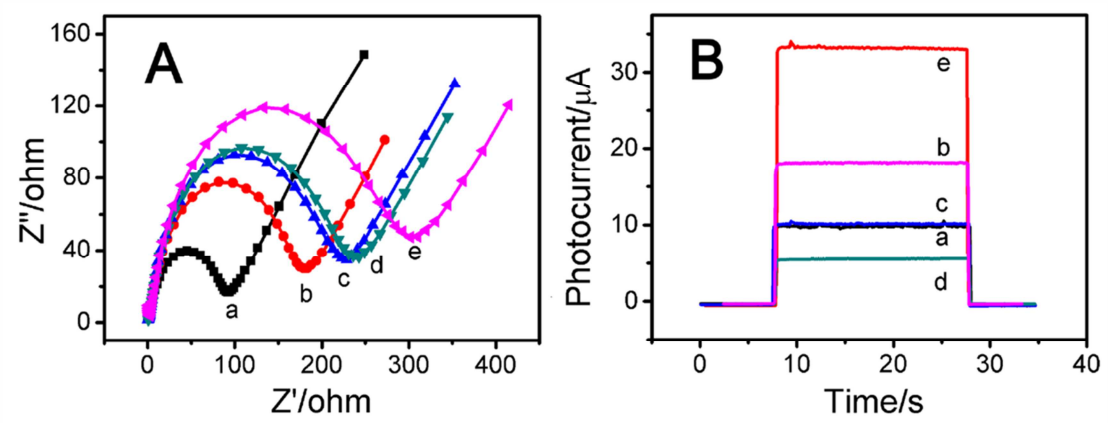

Figure 4. (A) EIS and (B) photocurrent responses of **(**a) g-C_3N_4/CdS QDs, (b) g-C_3N_4 /MoS_2/CdS QDs, (c) g-C_3N_4 /MoS_2/CdS QDs /MCH/c-DNA, (d) g-C_3N_4/MoS_2/CdS QDs/MCH/c-DNA/t-DNA_2, and (e) g-C_3N_4/MoS_2/CdS QDs /MCH/c-DNA/t-DNA_2/r-DNA/CdSe QDs.

Figure 5

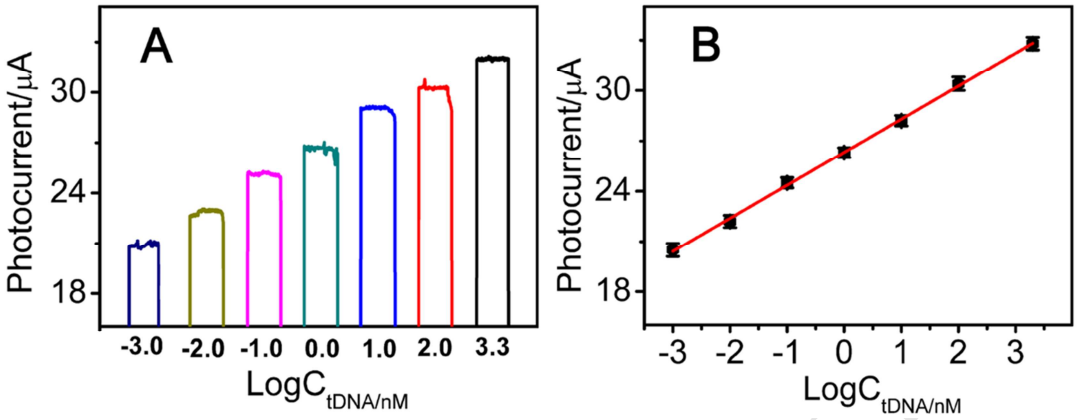

Figure 5. (A) Photocurrent responses of PEC DNA biosensor to different concentrations of t-DNA from 1 pM to 2 μM. (B) Calibration curve of the PEC DNA biosensor to t-DNA solution with various concentrations. The error bars display standard deviations of six parallel tests.

Figure 6

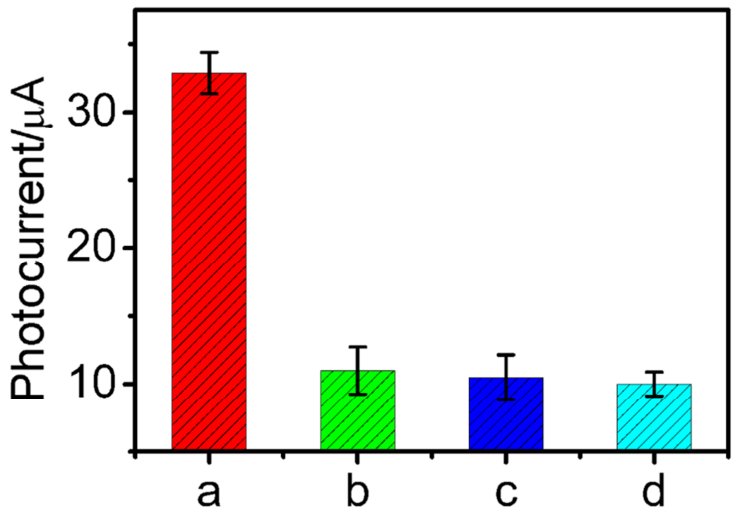

Figure 6. Photocurrent responses of the PEC DNA assay to 30 μL of 2 μM different DNA sequences. (a) t-DNA, (b) one-base mismatch DNAI, (c) three-base mismatch DNAII and (d) non-complementary DNA.

Table 1. Comparison of our PEC DNA bioassay with other detection methods.

Analytical Method	Detection Scope	LOD	Reference
PEC	1 pM-2 μM	0.32 pM	This work
PEC	0.01 nM-10.26 nM	1 pM	43
Colorimetric	0.4 nM-50 nM	0.2 nM	44
Colorimetric	0-120 nM	10 nM	45
Light Scattering	0.05 nM-100 nM	10 pM	46
Fluorescent	5.0 nM-175 nM	0.2 nM	47
Electrochemiluminescence	0.2 nM-100 nM	0.02 nM	48

Highlights

1. A novel enhanced photoelectrochemical DNA biosensor based on a compact heterojunction g-C_3N_4/MoS_2 and co-sensitization effect with CdSe QDs was constructed for ssDNA detection.

2. The biosensor adopts co-sensitive amplification technique.

3. The proposed photoelectrochemical protocol presented excellent selectivity.